Rab11-FIP3 links the Rab11 GTPase and cytoplasmic dynein to mediate transport to the endosomal-recycling compartment

Conor P. Horgan[1], Sara R. Hanscom[1], Rushee S. Jolly[2], Clare E. Futter[2] and Mary W. McCaffrey[1,*]

[1]Molecular Cell Biology Laboratory, Department of Biochemistry, Biosciences Institute, University College Cork, Cork, Ireland
[2]Division of Cell Biology, Institute of Ophthalmology, University College London, London EC1V 9EL, UK
*Author for correspondence (m.mccaffrey@ucc.ie)

Accepted 19 October 2009
Journal of Cell Science 123, 181-191 Published by The Company of Biologists 2010
doi:10.1242/jcs.052670

Summary

Several protein families control intracellular transport processes in eukaryotic cells. Here, we show that the Rab11 GTPase effector protein Rab11-FIP3 (henceforth, FIP3) directly interacts with the dynein light intermediate chain 1 (DLIC-1, gene symbol *DYNC1LI1*) subunit of the cytoplasmic dynein 1 motor protein complex. We show that Rab11a, FIP3 and DLIC-1 form a ternary complex and that DLIC-1 colocalises with endogenous FIP3 and Rab11a in A431 cells. We demonstrate that association between FIP3 and DLIC-1 at the cell periphery precedes minus-end-directed microtubule-based transport, that FIP3 recruits DLIC-1 onto membranes, and that knockdown of DLIC-1 inhibits pericentrosomal accumulation of key endosomal-recycling compartment (ERC) proteins. In addition, we demonstrate that expression of a DLIC-1-binding truncation mutant of FIP3 disrupts the ability of ERC proteins to accumulate pericentrosomally. On the basis of these and other data, we propose that FIP3 links the Rab11 GTPase and cytoplasmic dynein to mediate transport of material from peripheral sorting endosomes to the centrally located ERC.

Key words: FIP3, Rab11, dynein, DLIC-1, Rab11-FIP3, DLIC, DYNC1LI1

Introduction

Receptor-mediated endocytosis involves the internalisation of specific extracellular molecules (ligands) following their binding to specific receptors located on the cell surface (Maxfield and McGraw, 2004). Material that enters cells by this means is typically delivered to a peripheral organelle with tubulovesicular morphology known as the sorting endosome (Maxfield and McGraw, 2004). From sorting endosomes, cargo destined for degradation, such as growth factors and their receptors, are sorted to late endosomes for onward transport to lysosomes; conversely, many nutrient-binding ligands and their receptors are returned to the cell surface for repeated cycles of use. Material can be returned to the cell surface either directly from peripheral sorting endosomes (the fast recycling pathway) or indirectly by accessing the endosomal-recycling compartment (ERC) (the slow recycling pathway). The ERC has tubulovesicular morphology and, in many cell types, is clustered around the centrosome or microtubule-organising centre (MTOC) (Maxfield and McGraw, 2004).

Transport between compartments in the endosomal system is highly regulated and occurs through the formation of transport intermediates (membranous vesicles or tubules). Members of the Rab11 GTPase subfamily [Rab11a, Rab11b and Rab11c (also known as Rab25)] are enriched on the cytosolic face of the ERC and have emerged as key regulators of membrane trafficking through this organelle (Schlierf et al., 2000; Ullrich et al., 1996). Rab11 GTPases act through the recruitment of downstream effector proteins, prominent among which are a family of Rab11-interacting proteins termed the Rab11-FIPs, or FIPs (Horgan and McCaffrey, 2009). During interphase, FIP3 – a member of this protein family that is alternatively named eferin and arfophilin (Prekeris et al., 2001; Shin et al., 1999) – localises to the ERC and is required for structural integrity and pericentrosomal positioning of the ERC (Horgan et al., 2007; Horgan et al., 2004; Inoue et al., 2008). FIP3 also appears to function during cell motility (Jing et al., 2009) and, as cells divide, FIP3 is involved in membrane delivery from the ERC to sites of membrane insertion on the cleavage furrow and/or midbody (Horgan et al., 2004; Wilson et al., 2005).

Eukaryotic cells utilise mechanochemical forces generated by molecular motor proteins to move and position membranous compartments and their intermediates along an underlying cytoskeleton (Allan and Schroer, 1999; Cole and Lippincott-Schwartz, 1995; Soldati and Schliwa, 2006). One such molecular motor protein is cytoplasmic dynein 1 (henceforth, dynein), a minus-end-directed microtubule-based motor protein complex composed of heavy chains (HC), intermediate chains (IC), light intermediate chains (LIC) and light chains (LC) (King, 2000). Indeed, disruption of dynein function perturbs the distribution and function of various compartments in both the endocytic and biosynthetic pathways (Burkhardt, 1998; Burkhardt et al., 1997; Harada et al., 1998; Palmer et al., 2009; Traer et al., 2007).

A crucial facet in the study of membrane trafficking is the elucidation of the molecular details of how transport specificity is ensured; this includes determination of how membrane trafficking machinery is linked to motor proteins. Equally important is clarification of the functional outcomes of identified motor-cargo interactions. Here, we report that the Rab11 GTPase effector protein FIP3 interacts with a component of the dynein motor complex and demonstrate that this molecular interaction serves to drive membrane trafficking from peripheral sorting endosomes to the centrally located ERC.

Journal of Cell Science

Results

Exogenous FIP3 expression dramatically alters the distribution of the dynein motor complex condensing it into the FIP3-positive ERC through a direct interaction with DLIC-1

We have previously demonstrated that disruption of FIP3 function by RNAi or dominant-negative mutant expression results in the loss of the ERC from the pericentrosomal region of the cell (Horgan et al., 2007). Whereas these data clearly demonstrated the crucial importance of FIP3 for ERC homeostasis, the precise molecular details of how FIP3 performs this cellular function have remained unclear. One hypothesis we suggested was that FIP3 interacts either directly or indirectly with a minus-end-directed microtubule-based motor protein (Horgan et al., 2007). To test this, we examined the consequences of exogenous FIP3 expression on the subcellular distribution of the endogenous dynein motor protein complex. We have previously established that exogenous FIP3 localises to the pericentrosomal Rab11-positive ERC and that its expression dramatically condenses this compartment (Horgan et al., 2004; Horgan et al., 2005). In A431 cells exogenously expressing GFP-fused FIP3 and immunolabelled for distinct subunits of the dynein motor complex, we found that there was strong colocalisation between FIP3 and all dynein subunits tested (Fig. 1A). Furthermore, we also observed a dramatic accumulation of the dynein motor complex in the FIP3-positive ERC (Fig. 1A, compare transfected and non-transfected cells). To determine whether FIP3 can directly interact with the dynein motor complex, we used far-western blotting to investigate the ability of FIP3 to bind dynein light intermediate chain 1 (DLIC-1), a known cargo-binding subunit of the dynein motor complex (Bielli et al., 2001; Malone et al., 2003; Purohit et al., 1999; Sivaram et al., 2009). For these experiments, bacterial lysates induced to express His_6 fusions of the FIPs were resolved by SDS-PAGE, transferred to nitrocellulose and challenged with purified recombinant GST-fused DLIC-1. Bound protein was revealed with an anti-GST antibody. The data revealed a direct interaction between FIP3 and DLIC-1 (Fig. 1B). This interaction is specific because GST protein alone did not bind (note: a weak non-specific band is observed in all lanes) (Fig. 1C). Furthermore,

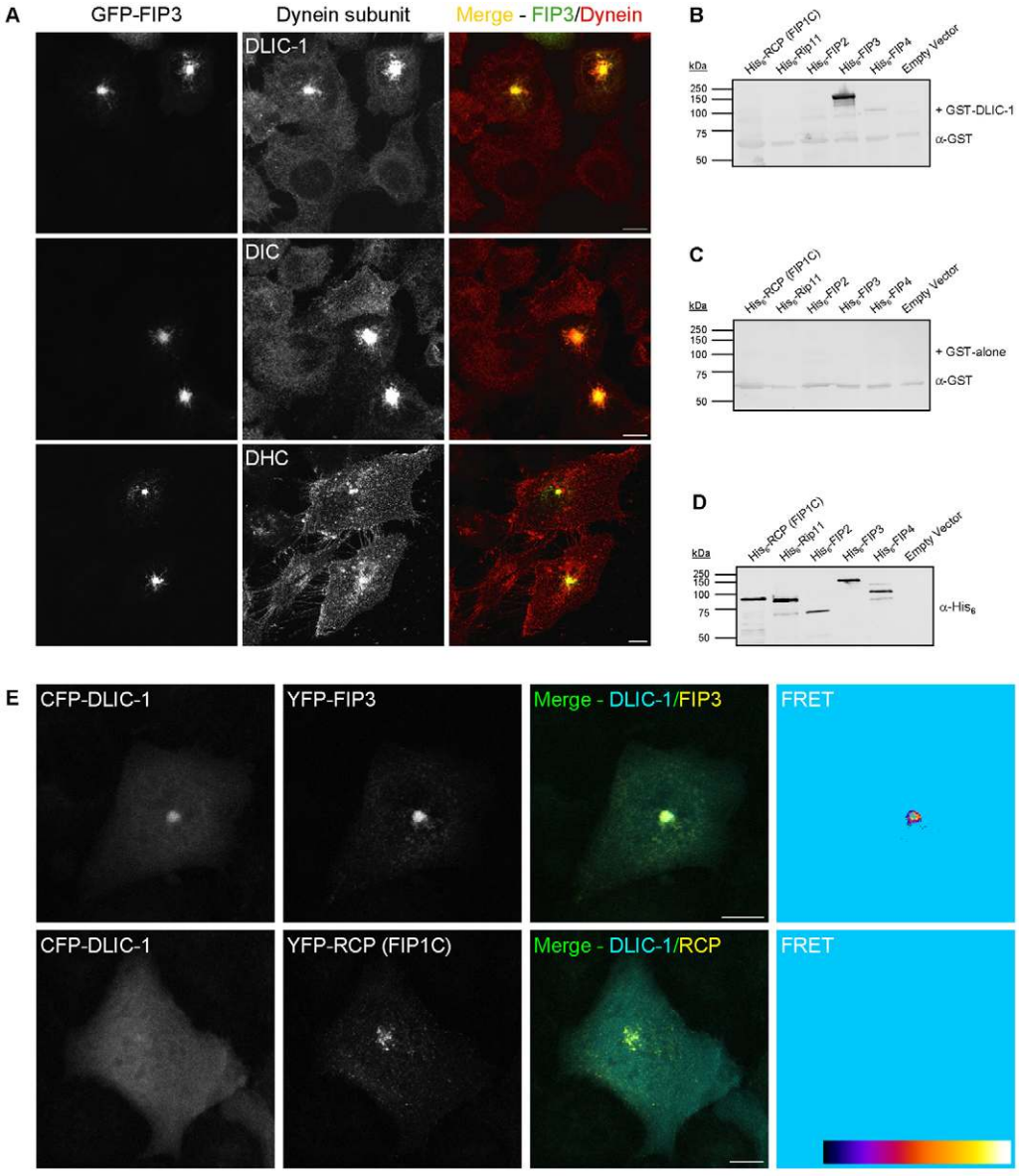

Fig. 1. FIP3 directly interacts with DLIC-1 in vitro and in vivo and increased expression of FIP3 perturbs dynein motor complex distribution. (**A**) A431 cells were transfected with pEGFP-C1/FIP3. At 16-18 hours post-transfection, cells were processed for immunofluorescence microscopy and immunostained with antibodies to detect endogenous DLIC-1, DIC or DHC. Images were acquired by confocal microscopy. Scale bar: 10 μm. (**B**,**C**) Far-western blot analysis of the ability of GST-DLIC-1 and GST alone to bind the FIPs. Bacterial lysates induced to express His_6 fusions of the FIPs or the empty vector were resolved by SDS-PAGE and transferred to nitrocellulose. The blots were then blocked, challenged with GST-DLIC-1 (B) or GST alone (C), washed, and bound protein revealed with an anti-GST antibody. (**D**) Western blot analysis of bacterial lysates induced to express His_6 fusions of the FIPs or the empty vector. The blot was revealed with an anti-His_6 antibody. (**E**) A431 cells were transfected with pECFP-C1/DLIC-1 and pEYFP-C1/FIP3 or pEYFP-C1/RCP. At 16 hours post-transfection, cells were fixed and processed for fluorescence microscopy. Images were acquired by confocal microscopy and FRET images generated. The FRET images display intensities of acceptor emission due to FRET in each pixel such that blue is no FRET and red is high FRET. Scale bar: 10 μm. These data are typical of at least three independent experiments.

GST-DLIC-1 did not bind any of the other FIPs (Fig. 1B), despite similar loading levels of the FIPs (Fig. 1D).

Our far-western blotting data demonstrates that DLIC-1 specifically binds FIP3 in vitro. To determine whether DLIC-1 directly interacts with FIP3 in vivo we investigated the ability of CFP-DLIC-1 to bind YFP-FIP3 by fluorescence resonance energy transfer (FRET). We detected a high degree of FRET between CFP-DLIC-1 and YFP-FIP3 in the pericentrosomal region of A431 cells that was specific because no FRET was detected between CFP-DLIC-1 and YFP-RCP (FIP1C) – another member of the FIP family (Fig. 1E). Additionally, in cells expressing CFP-DLIC-1 and YFP-FIP3, a significant proportion of the CFP-DLIC-1 protein was concentrated on the FIP3-positive pericentrosomal ERC, whereas in cells expressing CFP-DLIC-1 and YFP-RCP the majority of CFP-DLIC-1 protein was present in the cytosol (Fig. 1E). Together, these data illustrate that DLIC-1 directly and specifically interacts with FIP3 and that DLIC-1 forms a complex with FIP3 in vivo.

The dynein motor complex has well-defined roles in the movement of cargo towards the minus-end of microtubules that are found at the MTOC. Because we had identified a direct interaction between FIP3 and DLIC-1, and given that FIP3 is required for pericentrosomal positioning of the ERC (Horgan et al., 2007), we considered it plausible that FIP3-dynein might mediate the trafficking of material from a peripheral location in the cell towards the pericentrosomal ERC. To test this hypothesis, we investigated if, and where, FIP3 and DLIC-1 colocalised within the cell. As illustrated above, exogenous expression of FIP3 perturbs DLIC-1 distribution; therefore, we examined the localisation of both proteins at the endogenous level. As our previously described DLIC-1 and FIP3 antibodies were both generated in rabbits (Bielli et al., 2001; Horgan et al., 2004), we generated a new anti-DLIC-1 antibody in sheep. This affinity-purified antibody specifically detected DLIC-1 in A431 cells, as assessed by western blot and immunofluorescence analyses (see supplementary material Fig. S1A,B). Furthermore, similar to the data obtained with our rabbit anti-DLIC-1 antibody in Fig. 1A, this antibody revealed the altered DLIC-1 staining pattern induced by exogenous FIP3 expression (see supplementary material Fig. S1C). Together, these data demonstrate that our sheep anti-DLIC-1 antibody specifically detects DLIC-1.

On examination of the subcellular distribution of endogenous FIP3 and DLIC-1 in A431 cells, we found that both proteins displayed a punctate vesicular pattern throughout the cell that is highly concentrated in a pericentrosomal location (Fig. 2). Strong colocalisation was visible between FIP3 and DLIC-1 (46.0±7.7% of all FIP3 colocalises with DLIC-1) in the pericentrosomal region (Fig. 2). Furthermore, colocalisation between FIP3 and DLIC-1 is also observed in peripheral locations in the cell (Fig. 2, arrows), indicating that FIP3 and DLIC-1 associate in areas of the cells distal from the microtubule minus-end.

Rab11a, FIP3 and DLIC-1 form a ternary complex, and Rab11a colocalises with DLIC-1

Given that FIP3 function on the ERC is Rab11-dependent (Horgan et al., 2007) and because FIP3 directly interacts with DLIC-1, we considered it plausible that Rab11a, FIP3 and DLIC-1 could form a ternary complex. To test this, we investigated by far-western blotting the ability of FIP3 to link constitutively active Rab11a (Rab11a Q70L) to DLIC-1. For these experiments, purified recombinant His_6-DLIC-1 was resolved by SDS-PAGE and transferred to nitrocellulose. Separate His_6-DLIC-1-containing blots were then challenged with purified recombinant GST alone, GST-Rab11a Q70L, or GST-Rab11a Q70L plus His_6-FIP3. Bound GST-fused protein was then revealed with anti-GST antibody. These data revealed that neither GST alone nor GST-Rab11a Q70L directly binds His_6-DLIC-1 (Fig. 3A). However, when His_6-FIP3 was added together with GST-Rab11a Q70L, GST-Rab11a Q70L bound strongly to the membrane (Fig. 3A, right panel). Because Rab11a Q70L cannot directly bind DLIC-1 these data illustrate that Rab11a, FIP3 and DLIC-1 can form a ternary complex and that FIP3 links Rab11a to DLIC-1. Next, we examined the distribution of endogenous Rab11a with respect to DLIC-1 in A431 cells. These experiments revealed that Rab11a colocalises with DLIC-1 (42.9±5.7% of Rab11a colocalises with DLIC-1) on punctate structures in pericentrosomal and peripheral locations in the cell (Fig. 3B).

FIP3 and DLIC-1 binding precedes minus-end-directed microtubule-based transport

We have previously reported that nocodazole-induced disruption of microtubules peripherally distributes the ERC (Horgan et al., 2004). In that study, we monitored endogenous FIP3 localisation to visualise the ERC. To investigate whether the exaggerated ERC structure induced by overexpression of FIP3 is also organised along the microtubule cytoskeleton, we treated A431 cells exogenously expressing GFP-FIP3 with either DMSO (solvent control) or DMSO-solubilised nocodazole. As expected, treatment of cells with nocodazole disrupted the microtubules and led to fragmentation and peripheral distribution of the FIP3-positive ERC (Fig. 4A). Interestingly, we found that the peripherally distributed FIP3-positive ERC was also positive for DLIC-1 (Fig. 4B), and, as

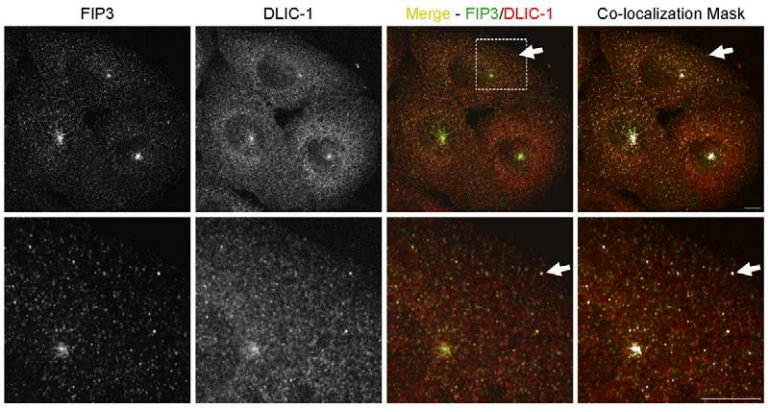

Fig. 2. FIP3 colocalises with DLIC-1 in central and peripheral and locations in the cell. A431 cells were processed for immunofluorescence microscopy and co-immunostained for FIP3 and DLIC-1 (sheep antibody). The boxed area is shown at higher magnification in the lower panels. Arrows point to yellow peripheral structures with colocalised proteins. Colocalisation is further illustrated by colocalisation mask analysis, which represents yellow pixels (overlapping regions of red and green) that have been extracted from the Merge images, converted to white and then superimposed on the Merge images. Images were acquired by confocal microscopy. Scale bar 10 μm. These data are typical of three independent experiments.

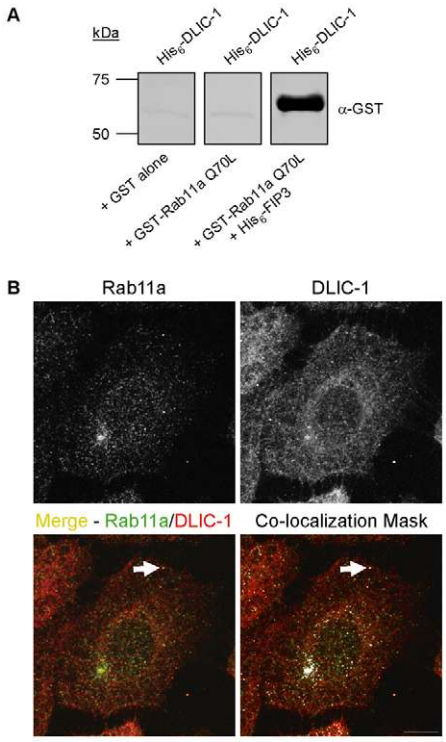

Fig. 3. Rab11a, FIP3 and DLIC-1 form a ternary complex and Rab11a colocalises with DLIC-1. (**A**) Far-western blot analysis of the ability of Rab11a Q70L, FIP3 and DLIC-1 to form a ternary complex. Purified recombinant His_6-DLIC-1 protein was resolved by SDS-PAGE and transferred to nitrocellulose. The blots were then blocked and challenged with either GST alone, GST-Rab11a Q70L or GST-Rab11a Q70L and His_6-FIP3. Blots were then washed, and bound protein revealed with an anti-GST antibody. (**B**) A431 cells were processed for immunofluorescence microscopy and co-immunostained for Rab11a and DLIC-1 (sheep antibody). Arrows point to yellow peripheral structures with colocalised proteins. Colocalisation is further illustrated by the colocalisation mask image. Images were acquired by confocal microscopy. Scale bar: 10 μm. These data are typical of at least three independent experiments.

expected, positive for ERC-marker proteins such as Rab11a and the transferrin receptor (TfnR) (data not shown).

To determine whether association between FIP3 and DLIC-1 precedes minus-end-directed microtubule-based transport, we investigated whether DLIC-1 could be recruited by peripherally localised exogenous FIP3 that was produced in cells subsequent to disruption of the microtubule cytoskeleton. For these experiments, A431 cells were left untreated or treated with nocodazole for 30 minutes to disrupt microtubules. Cells were then transfected for 6 hours with GFP-FIP3 in the absence (control) or continued presence of nocodazole before fixation and immunostaining. In control cells, we found that at 6 hours post-transfection, the exogenous protein displayed a typical pericentrosomal localisation pattern, which, as expected (see Fig. 1A), had compacted the DLIC-1 localisation (Fig. 4C, upper panels). Conversely, in cells transfected with GFP-FIP3 in the presence of nocodazole the exogenous FIP3 protein was found in peripheral structures, which also strongly immunostained for DLIC-1 (Fig. 4C, middle panels). Because these cells lack an intact microtubule cytoskeleton, these data suggest that DLIC-1 was recruited onto peripheral structures containing GFP-FIP3, which had been produced by the cells subsequent to the microtubule disruption. This indicates that an interaction between FIP3 and DLIC-1 precedes minus-end-directed transport along microtubules.

Because nocodazole-induced disruption of microtubules is reversible, we determined whether the peripheral structures positive for FIP3 and DLIC-1 could be transported to the pericentrosomal region of cells after the removal of nocodazole. In cells that were treated with nocodazole, then transfected with GFP-FIP3 for 6 hours in the presence of nocodazole, and finally washed and returned to fresh medium for 30 minutes before fixation and immunostaining, we found that material positive for FIP3 and DLIC-1 had been transported to the centrally located pericentrosomal region of the cell (Fig. 4C, lower panels). Together, these data illustrate that FIP3 and DLIC-1 can associate at peripheral locations in the cell, that this association precedes minus-end-directed microtubule-based endosomal transport and that, in the presence of intact microtubules, vesicles positive for FIP3 and DLIC-1 move towards the centre of the cell.

FIP3 recruits DLIC-1 onto membranes

The data presented above suggest that FIP3 might recruit the dynein complex onto endosomal membranes. To test this, we performed a protein recruitment assay whereby we determined if exogenous FIP3 was capable of recruiting purified recombinant DLIC-1 onto membranes. For these experiments, A431 cells expressing GFP-FIP3 were saponin-permeabilised prior to fixation and then incubated in reaction buffer containing purified recombinant His_6-fused DLIC-1. We found that the His_6-DLIC-1 protein was recruited onto GFP-FIP3-positive membranes, as evidenced by colocalisation between GFP-FIP3 and the recombinant DLIC-1 protein (Fig. 5, compare transfected and non-transfected cells in the upper panels). In addition, significantly increased His_6-DLIC-1 protein was observed in peripheral locations of GFP-FIP3-expressing cells (Fig. 5, upper panels). To examine the specificity of this result we determined whether GFP-RCP was also capable of recruiting His_6-DLIC-1 onto membranes and found that it could not (Fig. 5, lower panels). As further controls, we also determined if GFP-FIP4 could recruit His_6-DLIC-1 and if GFP-FIP3 could recruit another His_6-fused protein (the tail region of Myosin Vb) onto membranes and found that they could not (see supplementary material Fig. S2). Together, these data illustrate that FIP3 specifically recruits DLIC-1 onto endosomal membranes.

Suppression of DLIC-1 by RNAi prevents pericentrosomal accumulation of key ERC-marker proteins

Taken together, the data presented above, and that previously reported (Horgan et al., 2007), suggest that a complex formed between Rab11a, FIP3 and DLIC-1 might serve to traffic material from sorting endosomes towards the centrally located ERC. If this were the case, we hypothesised that depletion of DLIC-1 by RNAi should prevent pericentrosomal accumulation of ERC-marker proteins.

Significant reduction in DLIC-1 levels (knockdown) was achieved 72 hours post-transfection of A431 cells with DLIC-1 siRNA; as assessed by western blot [densitometry analyses indicate that 27.6±6.1% of the DLIC-1 protein remains in siRNA-treated cells (see supplementary material Fig. S3A)] and immunofluorescence microscopy [25±9.6% of cells retain some DLIC-1 staining (see supplementary material Fig. S3B)]. Interestingly, we found that both Rab11a and FIP3 displayed reduced pericentrosomal staining in A431 cells depleted of DLIC-1 (Fig. 6A,B). In addition, because the TfnR, and its ligand transferrin (Tfn), traffic through the ERC, we determined

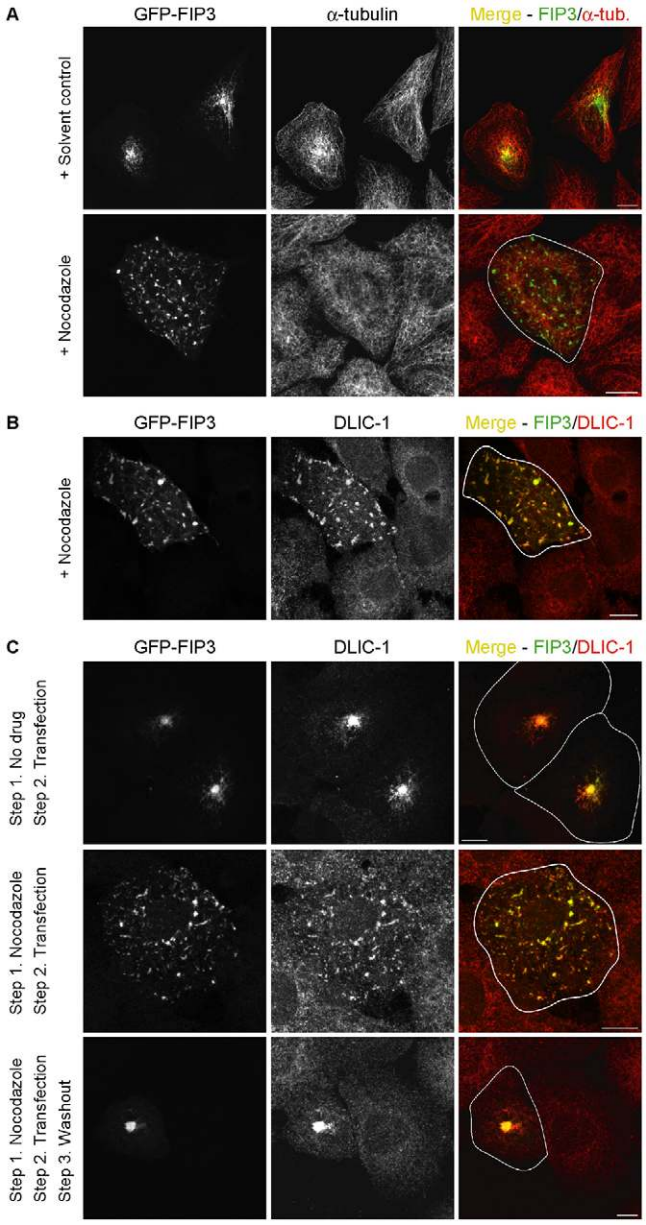

Fig. 4. Association between FIP3 and DLIC-1 precedes minus-end-directed microtubule-based transport. A431 cells were transfected with pEGFP-C1/FIP3. At 16-18 hours post-transfection, cells were treated with DMSO (solvent control) or nocodazole for 30 minutes and then processed for immunofluorescence microscopy and immunostained with antibodies to α-tubulin (**A**) or DLIC-1 (**B**). (**C**) Upper panels: A431 cells were transfected with pEGFP-C1/FIP3 and, 6 hours later, processed for immunofluorescence microscopy and immunostained with an antibody to DLIC-1. Middle panels: A431 cells were treated with nocodazole for 30 minutes to disrupt microtubules. Cells were then transfected with pEGFP-C1/FIP3 in the continued presence of nocodazole and, 6 hours later, processed for immunofluorescence microscopy and immunostained with an antibody to DLIC-1. Lower panels: A431 cells were treated with nocodazole for 30 minutes to disrupt microtubules and then transfected with pEGFP-C1/FIP3 in the continued presence of nocodazole. After 6 hours, cells were returned to fresh media (without nocodazole) for 30 minutes and then processed for immunofluorescence microscopy and immunostained with an antibody to DLIC-1. Individual transfected cell outlines are indicated with white lines. Images were acquired by confocal microscopy and are typical of at least three independent experiments. Scale bars: 10 μm.

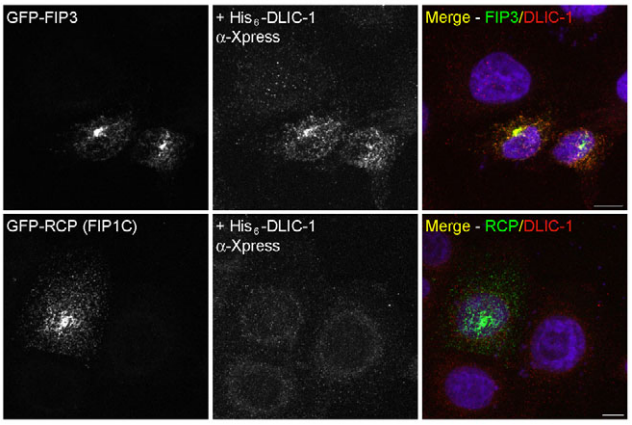

Fig. 5. FIP3 recruits DLIC-1 onto membranes. A431 cells were transfected with pEGFP-C1/FIP3 or pEGFP-C3/RCP. At 16 hours post-transfection, cells were saponin-permeabilised prior to fixation and incubated with purified recombinant His_6-DLIC-1. Cells were then processed for immunofluorescence microscopy and immunostained with an anti-Xpress antibody (the Xpress epitope is present in the His_6-DLIC-1 fusion protein). DAPI was used to visualise the nuclei. Images were acquired by confocal microscopy and are typical of three independent experiments. Scale bars: 10 μm.

whether endocytosed fluorophore-labelled Tfn was capable of accessing the pericentrosomal region of cells depleted of DLIC-1. We found that following 45 minutes of continuous internalisation of fluorophore-labelled Tfn, the Tfn failed to access the pericentrosomal region of DLIC-1-depleted cells (Fig. 6A,B). This result was corroborated by electron microscopy data. For electron microscopy experiments, A431 cells were treated with either control or DLIC-1 siRNA and incubated for 45 minutes in the presence of Tfn-conjugated horseradish peroxidase (HRP) (Tfn-HRP). The area surrounding the centrioles in all sections was then examined for the presence or absence of Tfn-HRP, which could be visualised as an electron-dense reaction product following incubation of the cells with diaminobenzidine (DAB) and hydrogen peroxide. Control cells displayed Tfn-HRP-positive small vesicles and tubules around the centrioles, indicative of the pericentrosomal ERC (Fig. 6C). By contrast, the area surrounding the centrioles in DLIC-1-depleted cells displayed minimal staining for Tfn-HRP, indicative of loss of the pericentrosomal ERC (Fig. 6C). To eliminate the possibility of off-target effects of the DLIC-1 siRNA, we investigated whether introduction of a plasmid encoding mouse DLIC-1 (which is not targeted by the siRNA directed against human DLIC-1) into cells depleted of human DLIC-1 was capable of reversing the knockdown phenotype. In cells expressing the recombinant mouse DLIC-1 protein, we found that endocytosed fluorophore-labelled Tfn could reach and concentrate at the pericentrosomal region of the cell, thus reversing the knockdown phenotype and indicating that the effects of human DLIC-1 siRNA were indeed specific (Fig. 6D,E). Together, these data indicate that DLIC-1 is necessary for pericentrosomal accumulation of its interacting partner FIP3, the key ERC-marker protein Rab11a, and ERC-cargo molecules such as Tfn.

Expression of a DLIC-1-binding truncation mutant of FIP3 disrupts trafficking to the ERC

Although the data presented above, and described previously (Horgan et al., 2007; Ullrich et al., 1996), clearly indicate that Rab11, FIP3 and DLIC-1 are required for pericentrosomal accumulation

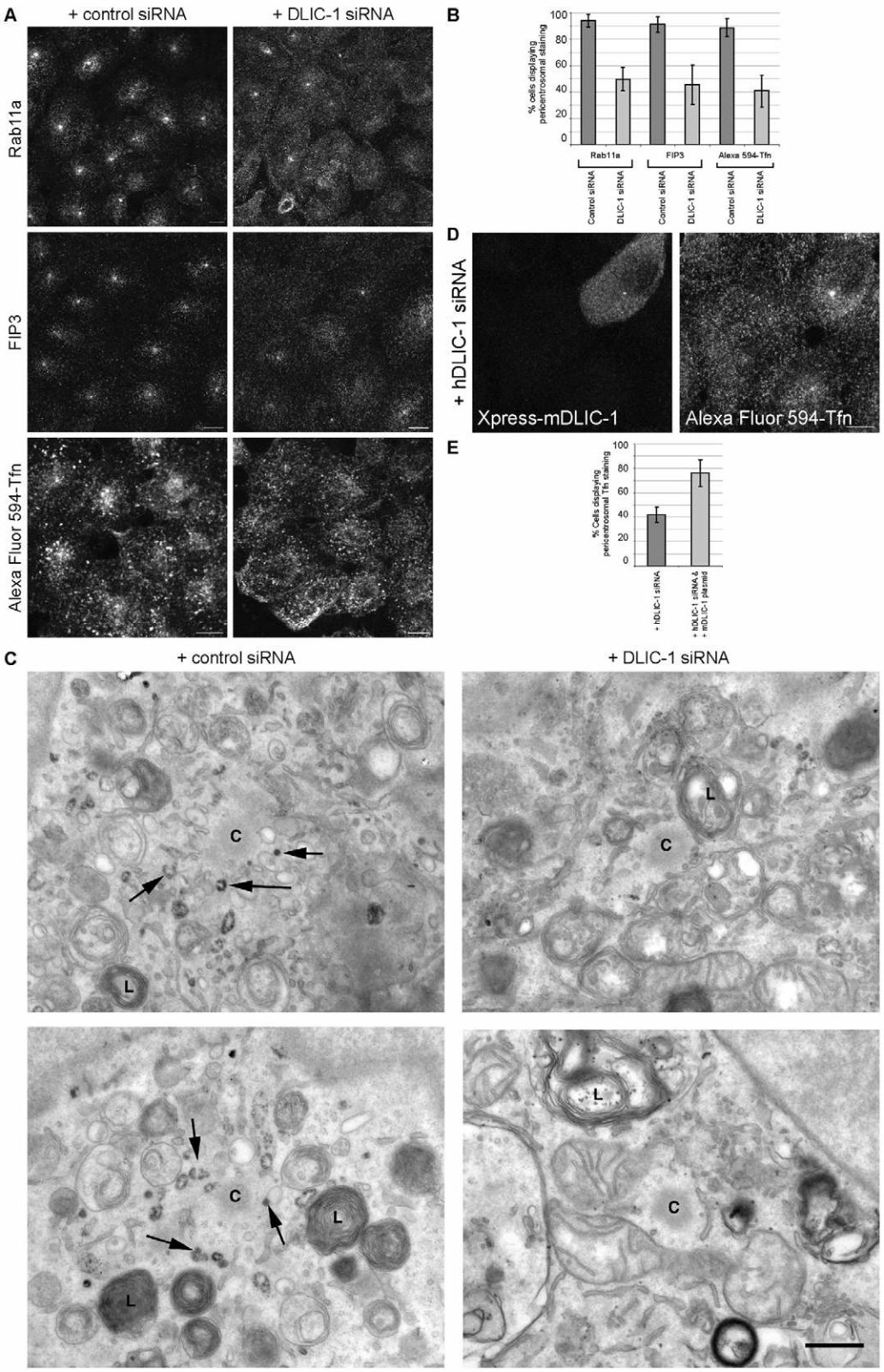

Fig. 6. Knockdown of DLIC-1 by RNAi prevents accumulation of key ERC-marker proteins in the pericentrosomal region of the cell. (**A**) A431 cells were treated with control or DLIC-1 siRNA. At 72 hours post-transfection, cells were either processed for immunofluorescence microscopy and immunostained with antibodies to Rab11a or FIP3, or allowed to internalise Alexa -Fluor-594-Tfn for 45 minutes at 37°C before being processed for fluorescence analysis. Scale bars: 10 µm. (**B**) Quantification of the proportion of cells displaying the knockdown phenotype. A minimum of 150 cells per experiment were analysed and the proportion of cells displaying pericentrosomal ERC-marker protein staining counted. Results are expressed as the mean percentages (from at least three independent experiments) ± s.d. (**C**) A431 cells were treated with control or DLIC-1 siRNA. At 72 hours post-transfection, cells were serum-starved before being allowed to internalise Tfn-HRP for 45 minutes at 37°C, and then processed for electron microscopy. Arrows indicate representative Tfn-HRP-containing structures. C, centrioles; L, lysosomes. Scale bar: 0.5 µm. (**D**) A431 cells were co-transfected with siRNA against human DLIC-1 (hDLIC-1) and plasmid DNA encoding Xpress-fused mouse DLIC-1 (mDLIC-1). At 72 hours post-transfection, cells were allowed to internalise Alexa-Fluor-594-Tfn for 45 minutes at 37°C before being processed for immunofluorescence microscopy and immunostained with anti-Xpress antibody. Scale bar: 10 µm. (**E**) Quantification of the proportion of cells displaying reversal of the knockdown phenotype after introduction of Xpress-fused mouse DLIC-1. A minimum of 125 cells per experiment were analysed and the proportion of cells displaying staining of pericentrosomal endocytosed Tfn counted. Results are expressed as the mean percentages (from three independent experiments) ± s.d.

of key ERC proteins they do not unambiguously demonstrate the importance of the interaction between FIP3 and DLIC-1 in mediating this trafficking step. To address this question, we mapped the region of FIP3 that interacts with DLIC-1 and generated a truncated FIP3 mutant protein to disrupt this interaction in vivo.

For these experiments, a series of constructs encoding FIP3 truncation mutants were generated (Fig. 7A), and their ability to bind DLIC-1 assayed by far-western blotting. Bacterial lysates induced to express His_6 fusions of wild-type and various FIP3 truncation mutants were resolved by SDS-PAGE and transferred to

nitrocellulose. This blot was then challenged with purified recombinant GST-fused DLIC-1 and the bound protein revealed with anti-GST antibody. These data revealed that, in addition to binding wild-type FIP3, DLIC-1 is capable of binding the Rab11-binding-deficient mutant of FIP3 (FIP3 I738E) (Horgan et al., 2007) (Fig. 7B). Furthermore, although DLIC-1 failed to bind the N-terminal 246 amino acids of FIP3, it was capable of interacting with amino acids 2-435 (Fig. 7B). Interestingly, DLIC-1 displayed no binding ability to FIP3 amino acids 247-756 or to the C-terminal 436-756 mutant [note: a weak band is observed in the $FIP3_{(247-756)}$ lane but not at the corresponding molecular weight of $FIP3_{(247-756)}$] (Fig. 7B). As controls, we confirmed that GST alone did not bind FIP3 wild-type or any FIP3 truncation mutants (note: a non-specific band is present in all lanes) (Fig. 7C) and that wild-type FIP3, and all FIP3 mutants proteins, were present at similar levels (Fig. 7D). Together, these data illustrate that DLIC-1 binds to FIP3 within the region of amino acids 2-435; this region is distinct from the C-terminal Rab11-binding domain of FIP3.

Next, we examined the effects of expression of the $FIP3_{2-435}$ truncation mutant on the ability of key ERC-marker proteins to accumulate in the pericentrosomal region of A431 cells. Because this mutant can bind DLIC-1, it would be expected that it should behave as an inhibitory polypeptide thus disrupting the physiological interaction between DLIC-1 and endogenous FIP3. As previously reported (Horgan et al., 2007), in cells expressing wild-type FIP3 we found that endocytosed Tfn was condensed into the pericentrosomal region, whereas in cells expressing FIP3 I738E (a FIP3 mutant unable to bind Rab11) Tfn failed to access the pericentrosomal region (Fig. 8A,D). Because FIP3 I738E retains its DLIC-1-binding ability (Fig. 7B), it is probable that it mediates this phenotype via its ability to bind endogenous DLIC-1. Interestingly, in cells expressing the $FIP3_{2-435}$ truncation mutant, endocytosed Tfn also failed to reach the pericentrosomal region (Fig. 8B,D). In addition, in cells expressing $FIP3_{2-435}$ and immunostained for Rab11a, the Rab11a staining was also almost completely absent from the central region of the cell (Fig. 8C,D). On the other hand, in cells expressing $FIP3_{2-246}$, both Rab11a and endocytosed Tfn were found in the pericentrosomal region (Fig. 8B-D). Because $FIP3_{2-246}$ cannot bind DLIC-1 (Fig. 7B), these data indicate that the effects observed when $FIP3_{2-435}$ is expressed are specific and are not due to any effects caused by expression of the N-terminal 246 amino acids of FIP3 or the GFP fusion tag. Taken together, these data indicate that the interaction between FIP3 and DLIC-1 functions to mediate trafficking towards the pericentrosomal ERC.

FIP3-positive structures move towards the pericentrosomal ERC

The data presented above support the contention that the Rab11-FIP3-dynein complex transports endosomal material from peripheral to central locations in the cell. To further explore this possibility, we monitored the localisation of GFP-FIP3 in A431 cells by time-lapse microscopy. We found that, although most of the GFP-FIP3 protein was present on the pericentrosomal ERC (Fig. 9), GFP-FIP3-positive vesicles and membrane tubules were continuously moving from peripheral locations in the cell towards the centrally located ERC (Fig. 9, arrows). These data are consistent with a role for FIP3 in the movement of material from peripheral locations in the cell towards the ERC. Notably, GFP-FIP3-positive vesicles and membrane tubules were also observed to move away from the ERC (see supplementary material Movie 1).

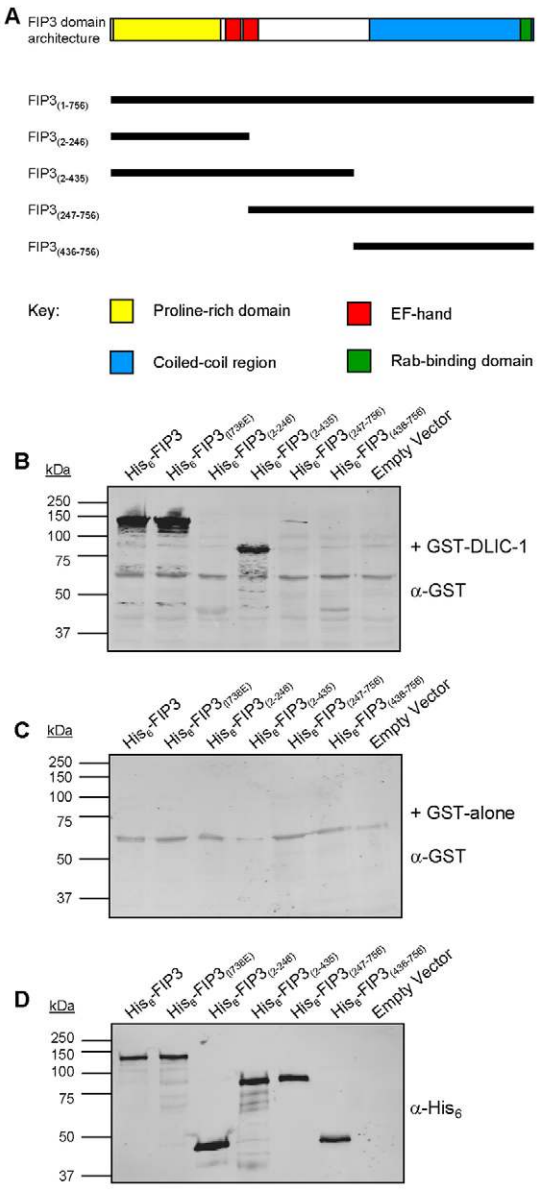

Fig. 7. The DLIC-1-binding region of FIP3 is distinct, and distant, from the Rab-binding domain. (**A**) Schematic representation of the domain architecture of FIP3 and the FIP3 truncation mutants analysed in this study. (**B**,**C**) Far western blot analyses of the ability of GST-DLIC-1 and GST alone to bind FIP3 truncation mutant proteins. Bacterial lysates induced to express His_6 fusions of wild-type FIP3, FIP3 truncation mutants or the empty vector were resolved by SDS-PAGE and transferred to nitrocellulose. The blot was then blocked, challenged with GST-DLIC-1 (B) or GST alone (C), washed, and bound protein revealed with an anti-GST antibody. (**D**) Western blot analysis of bacterial lysates induced to express His_6 fusions of wild-type FIP3, FIP3 truncation mutants or the empty vector. The blot was revealed with an anti-His_6 antibody. These data are typical of at least three independent experiments.

Discussion

Rab5, Rab4 and Rab11 are among the best characterised of all the Rab GTPases involved in endosomal trafficking. Rab5 functions in the early stages of endocytosis, whereas Rab4 and Rab11 regulate distinct endocytic-recycling pathways (Zerial and McBride,

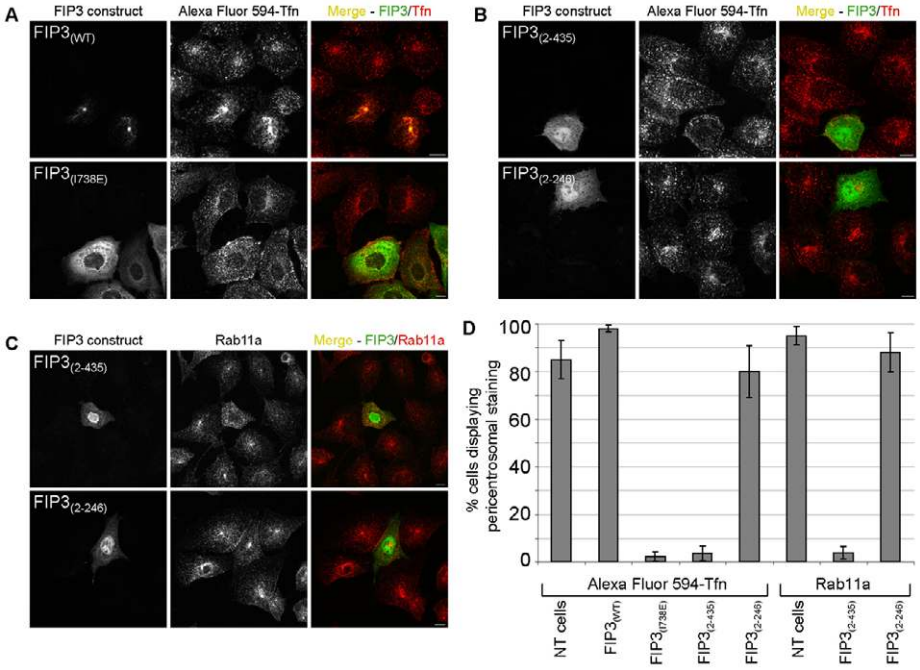

Fig. 8. Expression of a DLIC-1-binding truncation mutant of FIP3 prevents accumulation of key ERC-marker proteins in the pericentrosomal region of the cell. (**A-C**) A431 cells were transfected with constructs encoding GFP fusions of the indicated proteins. At 16-18 hours post-transfection the cells were allowed to internalise Alexa-Fluor-594-Tfn for 45 minutes at 37°C or processed for immunofluorescence microscopy and immunostained with anti-Rab11a antibodies. Images were acquired by confocal microscopy. Scale bar: 10 μm. (**D**) Quantification of the proportion of cells displaying the knockdown phenotype. A minimum of 150 cells per experiment were analysed and the proportion of cells displaying pericentrosomal ERC-marker protein staining counted. Results are expressed as the mean percentages (from at least four independent experiments) ± s.d.

2001). Although it is clear that Rab11 is involved in endosomal recycling during interphase (Ullrich et al., 1996), the entire details of the precise transport step(s) regulated by Rab11 have remained obscure. We have previously reported that the Rab11 effector protein FIP3 is necessary for the structural integrity and pericentrosomal positioning of the ERC (Horgan et al., 2007); however, the molecular details of how FIP3 mediates this Rab11-dependent cellular function remained unclear. Here, through the discovery of a direct interaction between FIP3 and the dynein motor complex, we provide evidence clarifying the molecular details of this aspect of FIP3 function. Specifically, we show that FIP3 directly interacts with the DLIC-1 subunit of the dynein complex and that this interaction serves to transport material from sorting endosomes to the ERC. On the basis of these and previously published data, we propose that FIP3 links the Rab11 GTPase and the dynein motor complex to transport material from peripheral sorting endosomes to the centrally located ERC (Fig. 10).

A considerable amount of supporting data on each of the molecules featured in this model has been described herein or previously reported. In the case of FIP3, disruption of its function by RNAi, or expression of a dominant-negative mutant that cannot bind Rab11, results in loss of all tested ERC-marker proteins from the pericentrosomal region of the cell (Horgan et al., 2007). Indeed, examination of the pericentrosomal region of FIP3-depleted cells by electron microscopy revealed an almost complete absence of tubular and vesicular elements in this region of the cell (Horgan et al., 2007). Conversely, we have shown here and previously (Horgan et al., 2004; Horgan et al., 2005), that overexpression of FIP3 results in dramatically increased accumulation of key ERC proteins (such as Rab11 and endocytosed Tfn) and the dynein motor complex in the pericentrosomal region of the cell. We also used RNAi studies to examine the involvement of FIP3 and DLIC-1 in Tfn recycling and found that their depletion does not inhibit Tfn recycling (see supplementary material Fig. S4). These results are consistent with previous studies (Horgan et al., 2004; Inoue et al., 2008) and are probably explained by a compensation by the fast direct recycling pathway in the absence of an FIP3-mediated or DLIC-1-mediated recycling route back to the cell surface via the ERC. Together, these data demonstrate that FIP3 is crucially required for the delivery of material to the pericentrosomal ERC and that exogenous expression of FIP3 drives the delivery of material to this cellular location.

At steady state, Rab11 is predominantly found on the pericentrosomal ERC (Ullrich et al., 1996); however, the model suggested above places some Rab11 transiently on sorting endosomes. Indeed, previous reports have indicated that a proportion of Rab11 localises to Rab5-positive, and Rab4-positive, sorting endosomes (Sonnichsen et al., 2000; Ullrich et al., 1996). In

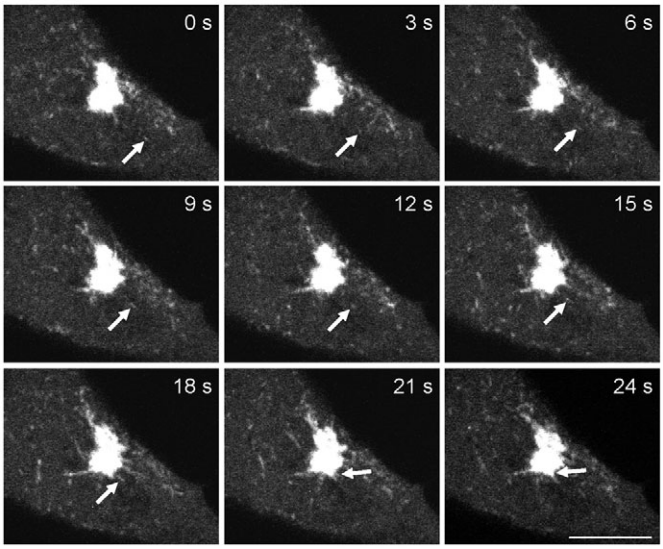

Fig. 9. FIP3-positive vesicles move towards the ERC. A431 cells were transfected with pEGFP-C1/FIP3 and time-lapse microscopy performed at 16 hours post-transfection. The arrows point to a single vesicle that was monitored over time at 3-second intervals. Scale bar: 10 μm.

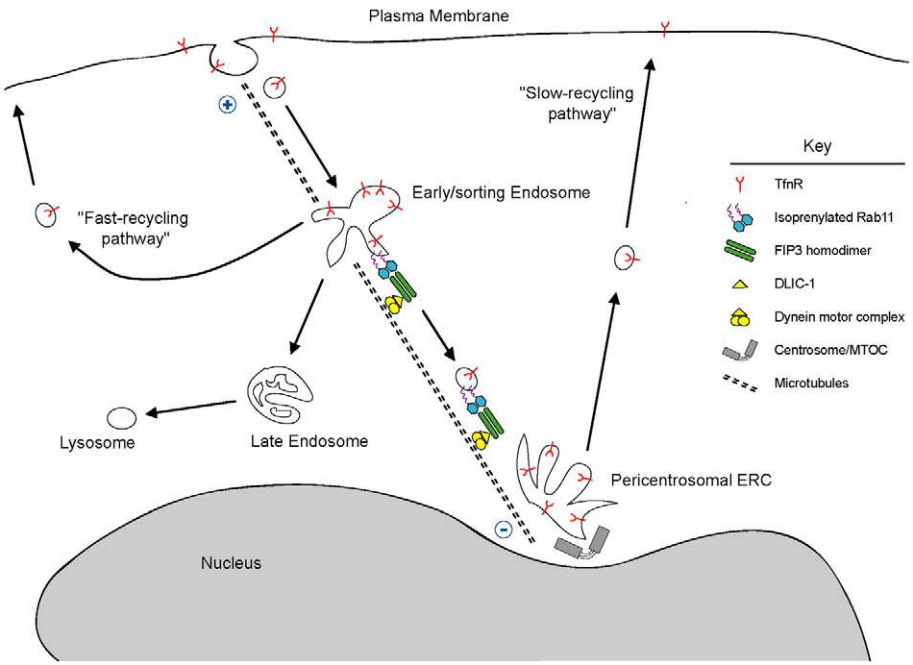

Fig. 10. Schematic model for the function of Rab11, FIP3 and DLIC-1 in endocytic trafficking during interphase. Following receptor-mediated endocytosis, the cargo in peripheral sorting endosomes, which is destined for the indirect slow-recycling pathway, is transported to the ERC in a Rab11-FIP3-dynein-motor-complex-dependent manner. This trafficking step involves the recruitment of FIP3 to sorting endosomes by active Rab11, leading to the formation of a heterotetrameric Rab11-FIP3 complex. This protein complex then recruits DLIC-1 via FIP3 and thus links the membrane-associated Rab11-FIP3 complex with the dynein motor complex. The dynein motor complex then moves cargo, such as Tfn-positive vesicles, to the pericentrosomal ERC, which is clustered around the MTOC (microtubule minus-end).

addition, we have found here that a proportion of Rab11a is found at peripheral locations in A431 cells, where it colocalises with DLIC-1. Furthermore, on the basis of Rab11 localisation and mutant expression studies in CHO and BHK cells, it was previously suggested that Rab11 might regulate trafficking from sorting endosomes to the ERC (Ullrich et al., 1996). In that work, expression of the dominant-negative Rab11 S25N mutant was found to inhibit Tfn transport to the ERC, cause dispersal of the Tfn-containing ERC, and result in accumulation of fluorophore-labelled Tfn in Rab5-positive sorting endosomes. We observed similar effects in A431 cells whereby expression of dominant-negative Rab11 S25N prevented pericentrosomal accumulation of endocytosed Tfn (data not shown). In addition, here and previously, we have demonstrated that expression of a Rab11-binding-deficient mutant of FIP3 (FIP3 I738E) prevents pericentrosomal accumulation of key ERC proteins (Horgan et al., 2007). Because FIP3 I738E can still bind DLIC-1, this indicates that Rab11 is required for the FIP3-dynein-mediated pericentrosomal accumulation of the ERC. Involvement of Rab11 in this trafficking step is also supported by further previously reported data whereby expression of the dominant-positive Rab11 Q70L mutant shifted the distribution of Tfn-labelled material towards the pericentrosomal region, with a consequential reduction in Tfn-labelled peripheral structures (Ullrich et al., 1996). This is consistent with increased trafficking from sorting endosomes to the pericentrosomal ERC in the presence of increased levels of active (GTP-bound) Rab11.

Considerable evidence also implicates dynein (the major molecular motor protein machinery that moves vesicular material towards the microtubule minus-end) in the trafficking of sorting endosomes to the ERC. The DLIC-1 subunit of dynein has previously been shown to partially localise to Rab4-positive sorting endosomes (Bielli et al., 2001) and we have found here by fluorescence and electron microscopy that knockdown of DLIC-1 prevents accumulation of endocytosed Tfn at the pericentrosomal region of the cell. Moreover, linking FIP3 and DLIC-1 in this trafficking step, we have demonstrated that expression of a dominant-negative DLIC-1-binding truncation mutant of FIP3 disrupts pericentrosomal accumulation of the ERC. We believe that this mutant acts by competing with endogenous FIP3 for DLIC-1-binding and thus disrupts the physiological interaction between endogenous FIP3 and DLIC-1. Although we tested several truncation mutants of DLIC-1 for FIP3-binding ability (see supplementary material Fig. S5), we were unable to identify the region of DLIC-1 that interacts with FIP3, and thus were unable to generate a dominant-negative DLIC-1 mutant. These findings suggest that the binding of DLIC-1 to FIP3 is more complex than simply through a single linear motif.

In further support of the model presented above, we found that FIP3 interacts with DLIC-1 in vivo, that Rab11a, FIP3 and DLIC-1 form a ternary complex, and that a proportion of DLIC-1 colocalises with FIP3 at peripheral locations in the cell. Further to this, we found that FIP3 recruits DLIC-1 onto membranes, that association between FIP3 and DLIC-1 precedes minus-end-directed transport along microtubules and that, in the presence of functional microtubules, FIP3-dynein complexes formed at peripheral locations in the cell move towards the pericentrosomal region. Finally, our time-lapse microscopy studies revealed that some FIP3-positive vesicles and tubules move from peripheral locations in the cell towards the ERC.

As outlined here, FIP3 binds a component of the dynein motor complex. Interestingly, FIP3 has also been reported to bind the plus-end-directed microtubule-based motor protein kinesin I (Simon and Prekeris, 2008). It is possible that during FIP3-mediated trafficking events, such as those defined during cytokinesis and cell migration and motility (Horgan et al., 2004; Jing et al., 2009; Wilson et al., 2005), FIP3 might become disassociated from dynein and instead engage with kinesin I to transport material towards the microtubule plus-end at the cleavage furrow or midbody in mitotic cells and/or at the leading edge of migrating cells. Interestingly, dissociation of dynein from FIP3 could be regulated by a phosphorylation-dephosphorylation cycle because DLIC-1 is known to be serine- and threonine-phosphorylated by the cdc2-cyclinB1 kinase during mitosis, an event believed to regulate membrane association of

dynein and lead to inhibition of organelle movement (Addinall et al., 2001; Dell et al., 2000; Niclas et al., 1996; Sivaram et al., 2009).

In summary, our data demonstrate that during interphase FIP3 serves as a linker protein between the Rab11 GTPase and the microtubule-based dynein motor complex to mediate the transport of material from peripheral sorting endosomes to the centrally located ERC. A major challenge that now remains is to determine how this trafficking step is regulated. This is currently a focus of ongoing research in our laboratory.

Materials and Methods

Plasmid construction

pEGFP-C1/FIP3, pEGFP-C1/FIP3 I738E, pEGFP-C3/RCP, pTrcHisC/FIP3, pTrcHisC/FIP3 I738E, pTrcHisC/FIP2, pTrcHisC/Rip11 and pTrcHisA/RCP have been previously described (Damiani et al., 2004; Horgan et al., 2007; Horgan et al., 2004; Horgan et al., 2005; Kelly et al., 2009; Lindsay and McCaffrey, 2004; Lindsay and McCaffrey, 2005). To generate pTrcHisC/FIP4 and pEGFP-C1/FIP4, FIP4 was amplified by PCR from an IMAGE clone (7939759) and inserted into the *Eco*RI site in pGEX-3X (GE Healthcare). The 1.9 kb *Eco*RI fragment from pGEX-3X/FIP4 was then subcloned into pTrcHisC (Invitrogen) and pEGFP-C1 (BD Biosciences). To generate pGEX-3X/DLIC-1, DLIC-1 was amplified by PCR from an IMAGE clone (40117391) and inserted into the *Eco*RI site in pGEX-3X. pTrcHisC/DLIC-1 was constructed by subcloning the 1.6 kb *Eco*RI fragment from pGEX-3X/DLIC-1 into pTrcHisC. pEGFP-C1/FIP3$_{(2\text{-}246)}$ was prepared by removal of the 1.6 kb *Bam*HI fragment from pEGFP-C1/FIP3. pEGFP-C1/FIP3$_{(2\text{-}435)}$ was prepared by removal of the 1.1 kb *Kpn*I fragment from pEGFP-C1/FIP3. pTrcHisA/FIP3$_{(436\text{-}756)}$ was generated by subcloning the 1.1 kb *Kpn*I-*Eco*RI fragment from pEGFP-C1/FIP3 into pTrcHisA (Invitrogen). pTrcHisB/FIP3$_{(2\text{-}435)}$ was generated by subcloning the 1.3 kb *Bgl*II-*Kpn*I fragment from pEGFP-C1/FIP3$_{(2\text{-}435)}$ into pTrcHisB (Invitrogen). pTrcHisB/FIP3$_{(247\text{-}756)}$ was generated by subcloning the 1.6 kb *Bam*HI-*Eco*RI fragment from pEGFP-C1/FIP3 into pTrcHisB. pTrcHisB/FIP3$_{(2\text{-}246)}$ was generated by subcloning the 0.8 kb *Bam*HI fragment from pTrcHisC/FIP3 into pTrcHisC. pGEX-3X/Rab11a Q70L was generated by subcloning the 0.8 kb *Bam*HI-*Eco*RI fragment from the previously described pTrcHisC/Rab11a Q70L construct (Horgan et al., 2007) into pGEX-3X. To generate pcDNA3.1HisC/mouse DLIC-1, mouse DLIC-1 was amplified by PCR from pCMV6-mouse DLIC-1 (Origene) and inserted into the *Xho*I site of pcDNA3.1HisC (Invitrogen). pECFP-C1/DLIC-1 was constructed by subcloning the 1.6 kb *Eco*RI fragment from pTrcHisC/DLIC-1 into pECFP-C1 (BD Biosciences). pEYFP-C1/FIP3 was constructed subcloning the 2.4 kb *Eco*RI fragment from pEGFP-C1/FIP3 into pEYFP-C1 (BD Biosciences). To generate pEYFP-C1/RCP, RCP was amplified by PCR from an expressed sequence tag template (EST # 3956619) and inserted into the *Bam*HI site of pEYFP-C1. Constructs generated by PCR were confirmed to be correct by double-strand sequencing.

Cell lines, nocodazole treatment, plasmid transfection and RNAi

The A431 (epidermal carcinoma) human cell line was cultured in Dulbecco's modified Eagle's medium supplemented with 10% (v/v) foetal bovine serum, 2 mM L-glutamine and 25 mM HEPES and grown in 5% CO_2 at 37°C. For nocodazole treatments, cells were incubated in medium containing 2 μM nocodazole (solubilised in DMSO). For overexpression studies, cells were transfected with plasmid constructs using Effectene (Qiagen) or TurboFect (Fermentas) as transfection reagents. FIP3 RNAi was previously described (Horgan et al., 2007). DLIC-1 expression in A431 cells was depleted by transfection with si*GENOME* SMARTpool reagents directed against DLIC-1 (Dharmacon) (20 pmol siRNA per well of a 24-well plate). As a control, cells were transfected with si*CONTROL* non-targeting oligonucleotides (Dharmacon). siRNA was transfected using Lipofectamine 2000 according to the manufacturer's instructions (Invitrogen).

Primary antibodies

Mouse monoclonal antibodies used were anti-DHC (Sigma), anti-DIC, anti-β-actin (Sigma), anti-poly-histidine (Sigma), anti-α-tubulin (Sigma), and anti-Xpress (Invitrogen). Commercial rabbit polyclonal antibodies used were anti-GST (Sigma) and anti-Rab11a (Zymed). Rabbit polyclonal anti-DLIC-1 and anti-FIP3 have been previously described (Bielli et al., 2001; Horgan et al., 2004). Sheep polyclonal anti-DLIC-1 was prepared by immunisation of a sheep with purified recombinant GST-fused DLIC-1 (immunisation was performed by the Scottish National Blood Transfusion Service). The resulting antiserum was affinity-purified against purified recombinant His_6-fused DLIC-1.

Recombinant protein purification

For purification of GST-DLIC-1 and GST-Rab11a Q70L, *E. coli* BL21 (DE3-RIL) cells were transformed with pGEX-3X/DLIC-1 or pGEX-3X/Rab11a Q70L. Single transformants were grown to an OD_{600}=1.0 and induced with 0.25 mM IPTG for 16 hours at 20°C. Recombinant proteins were then affinity-purified against glutathione-agarose (Sigma). For purification of His_6-DLIC-1, *E. coli* BL21 (DE3-RIL) cells were transformed with pTrcHisC/DLIC-1. A single transformant was grown to an OD_{600}=1.6 and induced with 1.0 mM IPTG for 16 hours at 20°C. Recombinant protein was then affinity-purified against Ni^{2+}-agarose beads (Qiagen). Purification of His_6-FIP3 has been described previously (Horgan et al., 2007).

Far-western blotting and immunoblotting

For far-western blotting, *E. coli* BL21 (DE3-RIL) cells containing the indicated constructs were induced to express recombinant protein as His_6 fusions with 0.1-1.0 mM IPTG (dependent on the construct) for 3 hours at 37°C. Samples, which had been normalised on the basis of the amount of His_6 fusion protein present, were then resolved by SDS-PAGE and transferred to nitrocellulose. In the case of the ternary complex formation experiments, 6.5 μg of purified recombinant His_6-DLIC-1 was resolved by SDS-PAGE and transferred to nitrocellulose. The nitrocellulose was then blocked with basic buffer (BB: 20 mM HEPES pH 7.5, 50 mM KCL, 10 mM $MgCl_2$, 1 mM DTT, and 0.1% Igepal CA-630) plus 5% nonfat dried milk for 12 hours at 4°C. The nitrocellulose was then incubated in interaction buffer (IB: BB plus 1% nonfat dried milk) containing 20 μg of indicated purified recombinant proteins for 4 hours at 4°C, washed with Tris-buffered saline containing 0.1% Tween-20, and the bound protein revealed by western blot with anti-GST antibody. Immunoblotting analyses were performed on an Odyssey Infrared Imaging System and processed using the Odyssey Infrared Imaging Application Software (LI-COR). Secondary antibodies used were IRDye 680 goat anti-rabbit and IRDye 680 goat anti-mouse (LI-COR) and IRDye 800 donkey anti-sheep (Rockland). The methodology for primary antibody immunoblotting was as previously described (Horgan et al., 2007).

Immunofluorescence and electron microscopy

Immunofluorescence microscopy was performed as described previously (Horgan et al., 2005). Secondary antibodies used were goat anti-mouse conjugated to Alexa Fluor 488 or 594 (Molecular Probes), goat anti-rabbit conjugated to Alexa Fluor 488 (Molecular Probes), donkey anti-rabbit conjugated to indocarbocyanine (Cy3) (Jackson ImmunoResearch), and donkey anti-sheep conjugated to Alexa Fluor 594 (Molecular Probes). DAPI (Sigma) was used to visualise nuclei. For Tfn-uptake experiments, cells were allowed to internalise Alexa-Fluor-594-coupled holo-transferrin (Molecular Probes) at 5 μg/ml for 45 minutes at 37°C before fixation. Images were recorded in a temperature-controlled environment (18°C) using a Zeiss LSM 510 META confocal microscope fitted with a 63× 1.4 plan apochromat lens. Colocalisation analyses were performed using the colocalisation module of the Zeiss LSM Image Examiner software. Colocalisation mask images represent overlapping high-intensity (intensity threshold was the same for all samples) green and red pixels that have been extracted from the merge images, converted to white and then superimposed on the merge images. Images were processed using Zeiss LSM Image Browser and Adobe Illustrator software. For quantification of colocalisation between the fluorescence signals obtained from co-stained samples, a minimum of seven randomly chosen cells were analysed. Percentage colocalisation between respective sets of proteins is presented as mean values from at least three independent experiments ± s.d. Colocalisation values were calculated by expressing the number of pixels in a given colocalisation mask as a percentage of total pixels for a given fluorophore. Electron microscopy studies were performed as described previously (Horgan et al., 2007).

Recruitment assay for His_6 fusion protein

A431 cells growing on glass coverslips were transfected with plasmids encoding GFP fusions of the indicated FIP proteins. At 16 hours post-transfection, the cells were washed with ice-cold reaction buffer (134 mM potassium acetate, 20 mM HEPES pH 7.4, 2.5 mM magnesium acetate) and permeabilised with reaction buffer containing 0.025% saponin for 15 minutes. Cells were then washed and overlaid with reaction buffer containing 0.5 mM ATP, 0.5 mM GTP, 25 μg/ml BSA, 1 mg/ml rat brain cytosol, 80 mM creatine phosphate, 1U/ml creatine kinase and 5 μg/ml of His_6-fused purified recombinant protein for 30 minutes at room temperature. Cells were then washed and processed for immunofluorescence analysis as described above. His_6 fusion proteins were detected using anti-Xpress antibodies. The Xpress epitope is present in the linker region of His_6 fusion proteins purified from the pTrcHis series of vectors (Invitrogen).

Transferrin-trafficking assay

A431 cells were grown on 13-mm round glass coverslips and treated with siRNA targeting the indicated proteins. At 60 hours post-transfection, the cells were allowed to continuously internalise Alexa-Fluor-594-coupled holo-transferrin at 5 μg/ml for 1 hour at 37°C. Cells were then either briefly washed with ice-cold PBS and immediately fixed with 3% PFA (loaded with labelled-Tfn) or washed with room temperature PBS and then incubated in fresh media containing 100-fold excess unlabelled holo-transferrin (Sigma) for 30 minutes and then washed and fixed (labelled-Tfn recycled). Samples were analysed on a Nikon E-600 epifluorescence microscope fitted with a Hamamatsu CCD C5985 camera. Twenty images from randomly selected fields were recorded (approximately 120 cells per image) from three independent experiments and the amount of fluorescence in the samples analysed using MetaMorph software (Molecular Devices). Average fluorescence levels in cells were then calculated and are presented as mean values ± s.d.

FRET

For FRET analysis, cells were transfected with CFP-fused DLIC-1 and with YFP-fused FIP3 or YFP-fused RCP. Images from fixed samples were recorded in a temperature-controlled environment (18°C) using a Zeiss LSM 510 META confocal microscope fitted with a 63× 1.4 plan apochromat lens. Colocalised FRET index images were generated using the FRET and Colocalisation Analyser plug-in (Hachet-Haas et al., 2006) run on ImageJ (NIH, Bethesda, MD; http://rsb.info.nih.gov/ij/.). The colocalised FRET images display intensities of acceptor emission due to FRET in each pixel, such that blue is no FRET and red is high FRET.

Time-lapse microscopy

A431 cells were plated on 35-mm glass bottom culture dishes (MatTek) and transfected with pEGFP-C1/Rab11-FIP3. At 16 hours post-transfection, the culture dishes were mounted on a Heater Insert P (CarlZeiss), maintained at 37°C, and images recorded at 3-second intervals using a Zeiss LSM 510 META confocal microscope fitted with a 63× 1.4 plan apochromat lens.

We dedicate this work to Anna Bielli who initiated the work on dynein in our laboratory and sadly passed away in 2006. The authors are grateful to all members of our laboratory for reagents and helpful discussion, Lavinia Bhatt for performing the MetaMorph analysis, and to Sylvie Urbé, David Stephens and Peter Cullen for useful discussions regarding this work. This work was supported by a BBSRC grant (BB/D011841; to C.E.F.) and a Science Foundation Ireland (SFI) investigator grant (05/IN.3/B859; to M.W.M.).

Supplementary material available online at
http://jcs.biologists.org/cgi/content/full/123/2/181/DC1

References

Addinall, S. G., Mayr, P. S., Doyle, S., Sheehan, J. K., Woodman, P. G. and Allan, V. J. (2001). Phosphorylation by cdc2-CyclinB1 kinase releases cytoplasmic dynein from membranes. *J. Biol. Chem.* **276**, 15939-15944.

Allan, V. J. and Schroer, T. A. (1999). Membrane motors. *Curr. Opin. Cell Biol.* **11**, 476-482.

Bielli, A., Thornqvist, P. O., Hendrick, A. G., Finn, R., Fitzgerald, K. and McCaffrey, M. W. (2001). The small GTPase Rab4A interacts with the central region of cytoplasmic dynein light intermediate chain-1. *Biochem. Biophys. Res. Commun.* **281**, 1141-1153.

Burkhardt, J. K. (1998). The role of microtubule-based motor proteins in maintaining the structure and function of the Golgi complex. *Biochim. Biophys. Acta* **1404**, 113-126.

Burkhardt, J. K., Echeverri, C. J., Nilsson, T. and Vallee, R. B. (1997). Overexpression of the dynamitin (p50) subunit of the dynactin complex disrupts dynein-dependent maintenance of membrane organelle distribution. *J. Cell Biol.* **139**, 469-484.

Cole, N. B. and Lippincott-Schwartz, J. (1995). Organization of organelles and membrane traffic by microtubules. *Curr. Opin. Cell Biol.* **7**, 55-64.

Damiani, M. T., Pavarotti, M., Leiva, N., Lindsay, A. J., McCaffrey, M. W. and Colombo, M. I. (2004). Rab coupling protein associates with phagosomes and regulates recycling from the phagosomal compartment. *Traffic* **5**, 785-797.

Dell, K. R., Turck, C. W. and Vale, R. D. (2000). Mitotic phosphorylation of the dynein light intermediate chain is mediated by cdc2 kinase. *Traffic* **1**, 38-44.

Hachet-Haas, M., Converset, N., Marchal, O., Matthes, H., Gioria, S., Galzi, J. L. and Lecat, S. (2006). FRET and colocalization analyzer-a method to validate measurements of sensitized emission FRET acquired by confocal microscopy and available as an ImageJ Plug-in. *Microsc. Res. Tech.* **69**, 941-956.

Harada, A., Takei, Y., Kanai, Y., Tanaka, Y., Nonaka, S. and Hirokawa, N. (1998). Golgi vesiculation and lysosome dispersion in cells lacking cytoplasmic dynein. *J. Cell Biol.* **141**, 51-59.

Horgan, C. P. and McCaffrey, M. W. (2009). The dynamic Rab11-FIPs. *Biochem. Soc. Trans.* **37**, 1032-1036.

Horgan, C. P., Walsh, M., Zurawski, T. H. and McCaffrey, M. W. (2004). Rab11-FIP3 localises to a Rab11-positive pericentrosomal compartment during interphase and to the cleavage furrow during cytokinesis. *Biochem. Biophys. Res. Commun.* **319**, 83-94.

Horgan, C. P., Zurawski, T. H. and McCaffrey, M. W. (2005). Purification and functional properties of Rab11-FIP3. *Methods Enzymol.* **403**, 499-512.

Horgan, C. P., Oleksy, A., Zhdanov, A. V., Lall, P. Y., White, I. J., Khan, A. R., Futter, C. E., McCaffrey, J. G. and McCaffrey, M. W. (2007). Rab11-FIP3 is critical for the structural integrity of the endosomal recycling compartment. *Traffic* **8**, 414-430.

Inoue, H., Ha, V. L., Prekeris, R. and Randazzo, P. A. (2008). Arf GAP ASAP1 interacts with Rab11 effector FIP3 and regulates pericentrosomal localization of transferrin receptor-positive recycling endosome. *Mol. Biol. Cell.* **19**, 4224-4237.

Jing, J., Tarbutton, E., Wilson, G. and Prekeris, R. (2009). Rab11-FIP3 is a Rab11-binding protein that regulates breast cancer cell motility by modulating the actin cytoskeleton. *Eur. J. Cell Biol.* **6**, 325-341.

Kelly, E. E., Horgan, C. P., Adams, C., Patzer, T. M., Ní Shúilleabháin, D. M., Norman, J. C. and McCaffrey, M. W. (2010). Class I Rab11-family interacting proteins are binding targets for the Rab14 GTPase. *Biol. Cell* **102**, 51-62.

King, S. M. (2000). The dynein microtubule motor. *Biochim. Biophys. Acta* **1496**, 60-75.

Lindsay, A. J. and McCaffrey, M. W. (2004). Characterisation of the Rab binding properties of Rab coupling protein (RCP) by site-directed mutagenesis. *FEBS Lett.* **571**, 86-92.

Lindsay, A. J. and McCaffrey, M. W. (2005). Purification and functional properties of Rab11-FIP2. *Methods Enzymol.* **403**, 491-499.

Malone, C. J., Misner, L., Le Bot, N., Tsai, M. C., Campbell, J. M., Ahringer, J. and White, J. G. (2003). The C. elegans hook protein, ZYG-12, mediates the essential attachment between the centrosome and nucleus. *Cell* **115**, 825-836.

Maxfield, F. R. and McGraw, T. E. (2004). Endocytic recycling. *Nat. Rev. Mol. Cell. Biol.* **5**, 121-132.

Niclas, J., Allan, V. J. and Vale, R. D. (1996). Cell cycle regulation of dynein association with membranes modulates microtubule-based organelle transport. *J. Cell Biol.* **133**, 585-593.

Palmer, K. J., Hughes, H. and Stephens, D. J. (2009). Specificity of cytoplasmic dynein subunits in discrete membrane-trafficking steps. *Mol. Biol. Cell* **20**, 2885-2899.

Prekeris, R., Davies, J. M. and Scheller, R. H. (2001). Identification of a novel Rab11/25 binding domain present in Eferin and Rip proteins. *J. Biol. Chem.* **276**, 38966-38970.

Purohit, A., Tynan, S. H., Vallee, R. and Doxsey, S. J. (1999). Direct interaction of pericentrin with cytoplasmic dynein light intermediate chain contributes to mitotic spindle organization. *J. Cell Biol.* **147**, 481-492.

Schlierf, B., Fey, G. H., Hauber, J., Hocke, G. M. and Rosorius, O. (2000). Rab11b is essential for recycling of transferrin to the plasma membrane. *Exp. Cell Res.* **259**, 257-265.

Shin, O. H., Ross, A. H., Mihai, I. and Exton, J. H. (1999). Identification of arfophilin, a target protein for GTP-bound class II ADP-ribosylation factors. *J. Biol. Chem.* **274**, 36609-36615.

Simon, G. C. and Prekeris, R. (2008). Mechanisms regulating targeting of recycling endosomes to the cleavage furrow during cytokinesis. *Biochem. Soc. Trans.* **36**, 391-394.

Sivaram, M. V., Wadzinski, T. L., Redick, S. D., Manna, T. and Doxsey, S. J. (2009). Dynein light intermediate chain 1 is required for progress through the spindle assembly checkpoint. *EMBO J.* **28**, 902-914.

Soldati, T. and Schliwa, M. (2006). Powering membrane traffic in endocytosis and recycling. *Nat. Rev. Mol. Cell. Biol.* **7**, 897-908.

Sonnichsen, B., De Renzis, S., Nielsen, E., Rietdorf, J. and Zerial, M. (2000). Distinct membrane domains on endosomes in the recycling pathway visualized by multicolor imaging of Rab4, Rab5, and Rab11. *J. Cell Biol.* **149**, 901-914.

Traer, C. J., Rutherford, A. C., Palmer, K. J., Wassmer, T., Oakley, J., Attar, N., Carlton, J. G., Kremerskothen, J., Stephens, D. J. and Cullen, P. J. (2007). SNX4 coordinates endosomal sorting of TfnR with dynein-mediated transport into the endocytic recycling compartment. *Nat. Cell Biol.* **9**, 1370-1380.

Ullrich, O., Reinsch, S., Urbe, S., Zerial, M. and Parton, R. G. (1996). Rab11 regulates recycling through the pericentriolar recycling endosome. *J. Cell Biol.* **135**, 913-924.

Wilson, G. M., Fielding, A. B., Simon, G. C., Yu, X., Andrews, P. D., Hames, R. S., Frey, A. M., Peden, A. A., Gould, G. W. and Prekeris, R. (2005). The FIP3-Rab11 protein complex regulates recycling endosome targeting to the cleavage furrow during late cytokinesis. *Mol. Biol. Cell* **16**, 849-860.

Zerial, M. and McBride, H. (2001). Rab proteins as membrane organizers. *Nat. Rev. Mol. Cell. Biol.* **2**, 107-117.